Mechanisms for Hydrogen-Atom Abstraction by Mononuclear Copper(III) Cores: Hydrogen-Atom Transfer or Concerted Proton-Coupled Electron Transfer?

Mukunda Mandal[†], **Courtney E. Elwell**[†], **Caitlin J. Bouchey**[†,‡], **Timothy J. Zerk**[‡], **William B. Tolman**[*,‡], **Christopher J. Cramer**[*,†]

[†]Department of Chemistry, Minnesota Supercomputing Institute, Chemical Theory Center, and Center for Metals in Biocatalysis, University of Minnesota, 207 Pleasant Street SE, Minneapolis, Minnesota 55455, United States

[‡]Department of Chemistry, Washington University in St. Louis, One Brookings Drive, Campus Box 1134, St. Louis, Missouri 63130, United States

Abstract

In a possibly biomimetic fashion, formally copper(III)–oxygen complexes LCu(III)–OH (1) and LCu(III)–OOCm (2) (L^{2-} = N,N'-bis(2,6diisopropylphenyl)-2,6-pyridinedicarboxamide, Cm = a,a-dimethylbenzyl) have been shown to activate X–H bonds (X = C, O). Herein, we demonstrate similar X−H bond activation by a formally Cu(III) complex supported by the same dicarboxamido ligand, LCu(III)–O_2CAr^1 (3, Ar^1 = *meta*-chlorophenyl), and we compare its reactivity to that of 1 and 2. Kinetic measurements revealed a second order reaction with distinct differences in the rates: 1 reacts the fastest in the presence of O−H or C−H based substrates, followed by 3, which is followed by (unreactive) 2. The difference in reactivity is attributed to both a varying oxidizing ability of the studied complexes and to a variation in X−H bond functionalization mechanisms, which in these cases are characterized as either a hydrogen-atom transfer (HAT) or a concerted proton-coupled electron transfer (cPCET). Select theoretical tools have been employed to distinguish these two cases, both of which generally focus on whether the electron (e^-) and proton (H^+) travel "together" as a true H atom, (HAT), or whether the H^+ and e^- are transferred in concert, but travel between different donor/acceptor centers (cPCET). In this work, we reveal that both mechanisms are active for X−H bond activation by 1−3, with interesting variations as a function of substrate and copper functionality.

Graphical Abstract

---

[*]**Corresponding Authors:** wbtolman@wustl.edu, cramer@umn.edu.

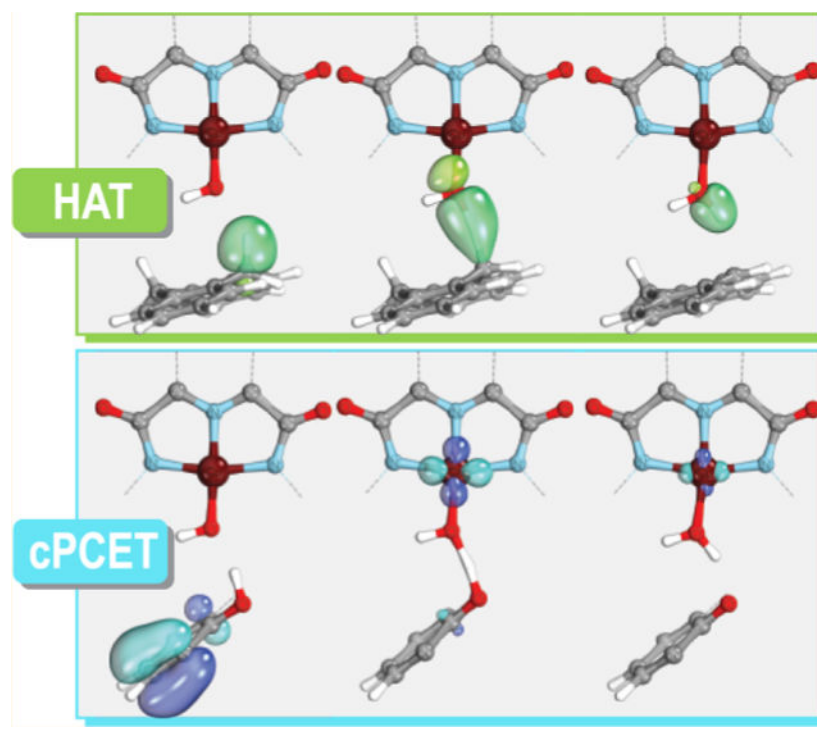The authors declare no competing financial interest.

INTRODUCTION

Copper is a key element in several enzymes that oxidize a variety of organic substrates.[1] Exploiting such reactivity for the controlled oxidation of light hydrocarbons is of special interest, as it has the potential to address challenges in fuel liquefaction.[2] Integral to understanding the reactivity of copper-based catalysts is the identification of reactive intermediates involved in the oxidative process.[3] Toward this end, mononuclear, formally Cu(III) cores supported by a tridentate dianionic ligand (N,N'-bis(2,6-diisopropylphenyl)-2,6-pyridinedicarboxamide, L^{2-})[3c,4] and derivatives[5] have been prepared as possible synthetic analogues of various putative copper–oxygen enzyme intermediates. The reactivity of selected [LCu(III)–Y] species (Y = OH, 1; Y = OOCm, 2; Cm = cumyl/a,a-dimethylbenzyl; Figure 1) for hydrogen atom abstraction (HAA) involving substrate X–H (X = C, O) bonds has been studied. For instance, 1 undergoes rapid HAA from substrates with weak C/O–H bonds,[4b,c] while 2 exhibits more limited reactivity toward similar substrates.[4d,e] Such differential reactivities dependent on the reactive ligand Y prompted us to explore in further detail how varying Y influences HAA reactions.

Transition-metal carboxylates are an additional class of compounds known for C–H bond functionalization.[6] Use of formally Cu(III)-carboxylates for this purpose, however, is unprecedented.[7] We report here the synthesis of a [Cu(III)–O_2CAr^1]$^{2+}$ core, 3, (Ar^1 = *meta*-chlorophenyl), supported by the same L^{2-} ligand as in 1 and 2. We systematically compare the HAA reactivities of 1, 2, and 3, toward the weak C–H bond in 9,10-dihydroanthracene (DHA) and the O–H bond in 2,4,6-tri-*tert*-butylphenol (Ar^3OH). We also apply a suite of computational techniques to gain insight into the underlying mechanistic details of these

various HAA processes involving DHA and 2,6-di-*tert*-butylphenol (Ar^{2}OH, which removes the para *t*-butyl group of Ar^{3}OH for computational convenience).

X–H bond activation by a [Cu(III)–Y]$^{2+}$ core formally involves the net transfer of both a proton (H$^+$) and an electron (e$^-$), i.e., the net transfer of a hydrogen atom. The mechanistic details with respect to "how" these transfers occur, however, can be complex, and a detailed understanding of reactivity and selectivity is critical if principles are sought for the design of new systems having tailored reactivity. Mechanistic behavior can, in principle, span a continuum of character, but discussion in terms of extremes offers heuristic value. Thus, one pair of contrasting limits for proton-coupled electron transfer involves (a) a *concerted* proton and electron transfer (CPET) process,[8] in which the electron and the proton are transferred in a single elementary step, and (b) a *stepwise* process that includes the generation of a (reactive) intermediate: either the proton transfer first, followed by electron transfer (PT/ET), or vice versa (ET/PT).[9]

CPET reactions themselves can also be discussed in terms of extremes, namely: (a) hydrogen-atom transfer (HAT) and (b) concerted proton-coupled electron transfer (cPCET). The nomenclature HAT generally describes CPET reactions where the electron and proton travel "together" between the same donor/acceptor sites, whereas the term cPCET is used to describe cases where the proton and electron are transferred in a single elementary step but they transfer between different donor and acceptor sites (Scheme 1).[9–12] Distinction of a cPCET reaction coordinate can also be made with regards to how closely the concerted reaction approaches the limiting stepwise paths (Scheme 1, edges) and invokes "asynchronicity" in e$^-$/H$^+$ transfer.[10,11b] Accordingly, a concerted asynchronous HAA reaction displaying a more PT-like character in the transition-state is referred to as a *basic* asynchronous cPCET mechanism, while that having a more ET-like character is usually designated as being *oxidatively* asynchronous.[13,14a]

HAA reactions following a CPET pathway avoid the formation of possible high-energy intermediates associated with elementary ET or PT,[9] but within the paradigm of CPET itself, it remains nontrivial to distinguish HAT from cPCET mechanisms, because both proceed as elementary processes with identical reactants and products.[15] In this regard, modern computational techniques can be powerful tools for characterization of a CPET reaction coordinate.[12,14,16] In this work, we apply multiple such diagnostic models to reveal that both HAT and cPCET mechanisms are associated with X–H bond (X = C, O) activation by [Cu(III)–Y]$^{2+}$ cores, with the particular mechanism varying as a function of the reactive ligand Y and the nature of the X–H substrate itself.

RESULTS AND DISCUSSION

Synthesis and Characterization of LCu(III)O$_2$CAr^1.

Reaction of a solution of [NBu$_4$][LCu(II)OH][4a] (1$'$) in tetrahydrofuran (THF) with *meta*-chlorobenzoic acid in the presence of 3 Å molecular sieves yielded teal-green [NBu$_4$][LCu(II)O$_2$CAr^1] (3$'$) (Scheme 2). The identity of this complex was confirmed by UV–vis (Figure S1) and EPR spectroscopy (Figure S2, Table S2), negative ion electrospray ionization mass spectrometry, CHN analysis, and X-ray crystallography (Table S1)

performed on an analogous NEt$_4^+$ salt (see Section 1 of Supporting Information (SI) for 3′ characterization information). The X-ray structure revealed a four-coordinate copper center with a distorted square-planar geometry (geometry index, τ_4 = 0.19; Figure 2).[17] The – O$_2$CAr^1 moiety is bound via one oxygen atom in the equatorial position at a short distance (1.929(3) Å) and via the second oxygen in the axial position at a longer distance (2.516(3) Å). Disregarding the latter weak interaction, the overall geometry and Cu–N distances for 3′ are similar to those of 1′ and [NBu$_4$][LCu(II)OOCm], 2′.[4d] However, the Cu–O distance is ~0.1 Å longer in 3′ than in 1′ and 2′, perhaps due to charge delocalization in the carboxylate moiety.

Cyclic voltammetry measurements were performed with 3′ in THF at 25 °C in the presence of 0.3 M electrolyte (NBu$_4$PF$_6$). A reversible process (i_{pa}/i_{pc} = 1.0, scan rate = 100 mV/s, E_p = 0.157 V vs Fc/Fc$^+$) was observed with half wave potential, $E_{1/2}$ = 0.228 V vs Fc/Fc$^+$ (Figure S3). This redox couple is ~0.3 V higher than previously reported LCu^{II}/LCu^{III} redox couples supported by anionic ligands (1′/1,[4a] $E_{1/2}$ = –0.074 V vs Fc/Fc$^+$; 2′/2[4d] = –0.154 V vs Fc/Fc$^+$) and ~0.5 V lower than for [LCu^{II}(THF)]$^{+/0}$ (0.735 V vs Fc/Fc$^+$) that features a neutral THF ligand.[4c] These results suggest that a stronger oxidant than those used for 1′ or 2′ is required to generate 3 chemically, and we chose acetyl ferrocenium tetrakis(3,5-bis(trifluoromethyl)-phenyl)borate, [AcFc][BAr$^F_4$], which has $E_{1/2}$ = 0.270 V vs Fc/Fc$^+$ in CH$_2$Cl$_2$[18].

UV–vis spectroscopy was used to monitor the one-electron oxidation of 3′ by [AcFc][BAr$^F_4$]. Upon addition of the oxidant at –80 °C in THF, two major features appeared. The growth of these features maximized after 1 equiv of [AcFc][BAr$^F_4$] had been added (Figure S4). The final spectrum of the intense blue solution contains a shoulder at 491 nm (ε = 5000 M^{-1} cm^{-1}) and features at 650 nm (ε = 13 000 M^{-1} cm^{-1}) and 830 nm (ε = 10 500 M^{-1} cm^{-1}). While the observation of these spectral features is clearly indicative of formation of a formally Cu(III) complex (3),[4a–d,5] the transitions themselves are significantly red-shifted compared to those observed for 1 (540 nm, ε = 11 500 M^{-1} cm^{-1}) and 2 (507 nm, ε = 13 000 M^{-1} cm^{-1}; 578 nm, ε = 12 000 M^{-1} cm^{-1}; 690 nm, ε = 9000 M^{-1} cm^{-1}) (Figure 3).[4] The oxidation of 3′ is chemically reversible at –80 °C in THF, as evident from experiments using repeated additions of oxidant ([AcFc][BAr$^F_4$]) and reductant (Fc*) (Figure S5). Further corrobo- rating the formulation of 3, the oxidized solution is EPR silent (Figure S6). Once generated, 3 is sufficiently stable at –80 °C to perform reactivity studies, but decays slowly via an ill-defined process ($t_{1/2}$ ~ 40 min, Figure S7).

Experimental Reactivity Studies.

The reactions of THF solutions of 1 and 3 (0.1 mM, both generated with 1 equiv [AcFc][BAr$^F_4$]) with excess (50 equiv) Ar^{3}OH (O–H bond- dissociation free energy, BDFE = 77.1 kcal mol^{-1})[9] at –80 °C were compared.[19] Consumption of 1 and 3 was indicated by decay of their UV–vis features; no such reaction was observed in the previous investigation of 2.[4d] Analysis of the product solutions after reactions of both 1 and 3 with Ar^{3}OH by EPR spectroscopy revealed a signal at g ~ 2 assigned to Ar^{3}O$^\bullet$ (~80% yield for 1,[4b] ~20% yield for 3, a low yield for which we have no clear explanation, see Figures S6 and S8–S9 for EPR data).[20] In addition to the organic radical, UV–vis data support formation of a Cu(II)

species we tentatively assign as LCu(II)(THF) on the basis of comparison to previously reported data (Figure S10).[4c] The kinetics for the reactions were followed by monitoring the decay of the reactant UV−vis spectral features. The resulting data were fit globally using a second order reaction model via ReactLab KINETICS;[21] the resulting rate constants shown in Table 1 are averages of triplicate measurements (see Figures S11−12 for kinetic data). The reaction of Ar^3OH with 3 ($k_2 = 3(1) \times 10^{-1}$ M^{-1} s^{-1}) was 2 orders of magnitude slower than with 1 ($k_2 = 2(1) \times 10^1$ M^{-1} s^{-1}) under the same reaction conditions. We explore possible rationales for this difference via theory below.

The reactivity of 3 with C−H bonds was also explored by examining the kinetics of reactions with DHA (BDFE = 76 kcal mol^{-1}).[9] No reaction was observed in the previous investigation of 2 with 200 equiv DHA at −25 °C in 1,2-difluorobenzene (1,2-DFB).[4d] Upon treatment of 3 with excess DHA (200 equiv) at −80 °C in THF, no enhancement of the rate of decay of 3 was observed. We then prepared 1 and 3 at higher temperature (−25 °C) in 1,2-DFB, a solvent that is less susceptible than THF to attack by 1 at that temperature. The UV−vis spectrum of 3 in 1,2-DFB at −25 °C (prepared with 1 equiv [AcFc][BAr^F_4], $t_{1/2}$ ~ 20 min) revealed slightly red shifted features (two major features appearing at 670 and 850 nm, respectively) compared to the analogous spectrum in THF. Treatment of the DFB solution of 3 with DHA (200 equiv) at −25 °C revealed a sluggish decay of the reactant UV−vis features and the growth of features due to anthracene (358 and 378 nm);[22] in a similar experiment using 10 equiv DHA, 0.6 equiv of anthracene was identified after workup and GC−MS analysis. The kinetic data were fit to a second order rate law, yielding $k_2 = 1.1(4) \times 10^{-1}$ M^{-1} s^{-1} (Table 1).[23] The reaction of 1 with DHA under the same conditions revealed $k_2 = 4.2(9) \times 10^1$ M^{-1} s^{-1}, which is within error of the previously reported value.[4c] Thus, the rate of reaction of 3 with DHA is ~2 orders of magnitude slower than that of 1 (see Figures S13−14 for kinetic data). In summary, distinct differences in the rates of reactions of 1, 2, and 3 with Ar^3OH and DHA were observed. Overall, 1 reacts the fastest in the presence of O−H or C−H bonds, followed by 3, which is followed by unreactive 2.

Computation Protocol.

In order to better understand the origin of the strongly red-shifted features in the UV−vis spectra of 3 compared to that of 1 and 2, explain the differential reactivity of the complexes toward a given substrate, and explore the underlying mechanism of various HAA processes, a detailed computational study employing density functional theory (DFT) was undertaken. Complete details of all computational methods, including benchmark studies addressing molecular geometries and electronic energies with various DFT models, can be found in the SI. The remaining text reports results from B3LYP density functional[24] calculations including Grimme's three-body dispersion term (D3)[25a] and Becke–Johnson (BJ) damping.[25b] For gas-phase geometry optimizations and vibrational frequencies, Pople's split-valence 6–31G(d) basis set[26] was used for light atoms and the Stuttgart/Dresden effective core potential with its associated basis set (SDD)[27] was used for Cu (basis-I). Improved electronic energies were computed from single-point calculations using the triple-ζ def2-TZVP basis set[28] for nonmetals and SDD basis and pseudopotential for Cu (basis-II). An experimentally relevant solvent reaction field was included in single-point calculations employing the SMD continuum solvation model[29] using solvent parameters for THF (ε =

7.4) in the case of reactions with Ar^2OH and for cyclopentanone ($\varepsilon = 13.6$, chosen to best mimic experimental 1,2-DFB ($\varepsilon = 13.8$)) in the case of DHA. For time-dependent density functional theory (TD-DFT) calculations, the PBE0 density functional[30] together with the def2-TZVP basis set for nonmetals and the def2-TZVPP basis and SDD pseudopotential for Cu was used (basis-III).

Although a seemingly technical computational detail, it is critical to note that all HAA reactions studied here involve closed-shell organic molecules and formally Cu(III) complexes ($3d^8$) as reactants, which are themselves also well-described by closed-shell singlet electronic states. Along all reaction coordinates, however, the reacting partners evolve into individual open-shell doublets (an organic radical and a formally Cu(II) ($3d^9$) species). Thus, within the single-determinantal Kohn–Sham (KS) DFT formalism, all reaction paths must at some point evolve on a broken-symmetry (BS) singlet potential energy surface (PES), characterized by KS determinants having $M_S = 0$ but $\langle S^2 \rangle$ values greater than 0 (and approaching 1 with increased separation of the radical partners).[31] We found that for all cases studied here, the crossing to the BS singlet PES occurs prior to reaching the transition-state (TS) structure for CPET. Thus, all TS structures were optimized at the unrestricted level of theory using the BS formalism (BS-UDFT), which takes the static correlation of the open-shell singlet into account in a cost-effective way.[32] Since the BS-UDFT determinant is contaminated by higher spin-states[32,33] (triplet in this case), an approximate spin-projection scheme proposed by Yamaguchi et al.[34] was used to spin-purify the final electronic energies.

Computed Spectra.

TD-DFT calculations were carried out for all three compounds 1–3 at the PBE0-D3(BJ)/basis-III/SMD(THF) level of theory on the B3LYP-D3(BJ)/basis-I optimized geometries to better understand the experimentally observed UV–vis spectral features. A qualitative picture of the electronic transitions was obtained by examining the KS orbitals, which, as Stowasser and Hoffmann have pointed out, are a good basis for qualitative interpretation of molecular orbitals and moreover have energy orderings consistent with more rigorous levels of theory.[35] Accordingly, the calculations indicated that the N-arylamide functionality of the L^{2-} ligand should be viewed as an extended π system with Lewis basicity concentrated in distinct regions, namely, the amide π-system and the aryl π-clouds (cf. the HOMO−5 and HOMO of 3, Figure 4). In every case, calculations suggest that pairs of low energy excitations into the lowest unoccupied molecular orbital (LUMO), which includes substantial Cu $d_{x^2-y^2}$ amplitude (Figure 4), are best described as ligand-to-metal charge transfer (LMCT) but coming as *combinations* from these two portions of the ligand, with varying degrees of aryl π versus amide π depending on the specific excitation. With respect to the red-shifted features for the benzoate case, this is entirely consistent with the more positive standard reduction potential for 3 ($E_{1/2}$ = 228 mV vs Fc/Fc$^+$) compared to that of 1 and 2 (−74 mV and −154 mV vs Fc/Fc$^+$, respectively).[4] Put differently, the Cu atom in 3 is more electrophilic, which is manifested in the orbital energies for 1 compared to 3: the HOMO energies are similar (within 0.07 eV), but the LUMO in 3 is much lower in energy (by ~0.40 eV), leading to the observed redshift (Table 2).

Unraveling Reactive Sites for HAA.

For complex 1, there is no ambiguity that the hydrogen atom from the substrate is transferred to the *O*-atom of the –OH functionality. For 2, by contrast, both the *O*-atom of the peroxo-moiety proximal to Cu (O^a) as well as the *O*-atom bonded to the cumyl benzylic position (O^b) may in principle be active (Figure 1). Similarly, for 3, HAA can occur at the carboxylate oxygen proximal to Cu (O^c) or at the more distal carbonyl *O*-atom (O^d) (Figure 1). To determine the active sites for HAA, we have characterized the reactivity at all four of these sites.

For 2, O^a is clearly the preferred site for HAA: computed activation free energies are lower by ~13 kcal/mol for Ar^2OH and ~6 kcal/mol for DHA compared to site O^b (Table 3). This trend is consistent with what would be expected based on alternative Cu-based product stabilities, i.e., a copper coordinated cumyl hydroperoxide versus a copper-oxo-coordinated cumyl alcohol, and indeed, the overall free energies of reaction (ΔG_0) for the 2/DHA pair are computed to be 3.9 and 18.6 kcal/mol at sites O^a and O^b, respectively (Figure S19). By contrast, HAA in 3 takes place preferentially at the distal site O^d, with free energies of activation lower by 8.7 and 4.5 kcal/mol for Ar^2OH and DHA, respectively, compared to reactivity at O^c (Table 3). This preference may also be attributed to product stability, with reaction at O^d leading to coordination of the more Lewis basic carbonyl of the product carboxylic acid to copper (Figures S18–19), but there may certainly also be some degree of steric influence (O^d being more accessible), particularly with the bulkier Ar^2OH substrate.

Comparative Reactivity with Ar^2OH and DHA.

Considering only lowest energy pathways, the calculated free energies of activation for 1–3 reacting with substrates Ar^2OH and DHA are presented in Table 4. For both substrates, we compute the reactivity order to be 1 > 3 > 2, which agrees with the experimentally observed trends (see Table 1 for comparison). Greater basicity of the hydroxyl group in 1, which results in a strong O–H BDFE in the product Cu(II) aqua complex and thus a strong thermodynamic driving force, plays a key role toward its highest reactivity. As the basicity of a carboxylate is low, the (perhaps surprisingly) higher reactivity of 3 than that of 2 can be attributed to its better oxidizing power as gauged by their respective $E_{1/2}$ values. Moreover, as discussed in more detail below, the higher reactivity of 3 may also be ascribed to a significant asynchronicity along the proton and electron transfer coordinates, since asynchronous transfer of H^+/e^-, together with other competing factors, has been demonstrated[36] to lower HAA activation barriers in other circumstances.

Mechanistic Diagnostics: Component of Dipole Moment along the Intrinsic Reaction Coordinate (IRC).

Having demonstrated a good correspondence between computed free energies of activation and experimentally measured rate constants, we may proceed to analyze the evolving electronic structures of the reacting partners along their respective reaction coordinates in order to better characterize the nature of the various reactions. As discussed above, in a cPCET process, the proton and electron travel between different donor/acceptor sites. Given the opposite charges of these particles, varying degrees of separation must affect the overall dipole moment, and in particular the component of the dipole moment projected on the

reaction coordinate vector, i.e., the X–H–Y axis.[16a] For an HAT mechanism, however, only a very small change in the projected dipole moment would be expected as the separation of the electron from the proton is never large.[16] Note that by focusing on the projection of the dipole moment onto the reaction coordinate (and its variation), quantitatively complicating factors associated with the magnitude and relative alignment of the *overall* dipole moment with the reaction coordinate are eliminated. Evolutions of the relevant components of the dipole moment along the reaction coordinate for HAA from Ar^2OH and DHA with complexes 1–3 are shown in Figure 5. The changes in the projected dipole moment for reactions of 1–3 with Ar^2OH (solid lines) range from 6 to nearly 25 D, consistent with the polar character of the O–H bonds involved and a cPCET process. By contrast, for 1 and 2, HAA from DHA (dashed-lines) proceeds with changes in the projected dipole moment of less than 5 D, consistent with a more "true" HAT process. Results for 3, however, are in striking contrast to those for 1 and 2: The change in the projected dipole moment for reaction with DHA is almost identical to that for reaction with Ar^2OH. This suggests a clear change in mechanism for HAA from DHA across the three [LCu(III)–Y] species: For Y = OH and OOCm an HAT pathway is followed, while for Y = O_2CAr^1 the mechanism is cPCET.

Mechanistic Diagnostics: Intrinsic Bond Orbital (IBO) Analysis.

In order to further characterize the HAA mechanism, we have employed the IBO localization scheme of Knizia and co-workers.[12,37] It has been demonstrated that changes in IBOs along a given reaction coordinate closely track the "curly arrows" generally used to explain bond-making/bond-breaking reaction mechanisms and, in the particular case of HAA reactions, for analyzing the nuances of HAT versus cPCET.[12,38] Illustrative examples are shown in Figure 6, where evolutions of IBOs for α- and β-electrons of breaking X–H bonds along the intrinsic reaction coordinate have been carefully assessed to understand relevant charge flow. Figure 6(a–c) shows evolution of the IBOs for the activated C–H bond during HAA from DHA by 1. In this simplest case, it is clear that along the reaction coordinate, the α-IBO (Figure 6(b), purple lobe) transforms from a C–H bond in DHA to an O–H bond in [LCu(II)–OH_2] as the electron follows the proton, while the β-IBO (Figure 6(c), green lobe) evolves from being a C–H bond to a semilocalized radical on the monohydroanthracene product. This electronic redistribution exemplifies a "true" HAT mechanism as shown in Figure 7(a).

A similar analysis for the reaction of 1 with Ar^2OH is shown in Figure 6(d–f). Evolution of the β-IBO of the O–H bond is shown in Figure 6(e), and the corresponding α-IBO evolves almost identically (Figure S20). Since *both* the α- and β-IBOs of the original O–H bond remain on the aryloxy substrate along the H-coordinate, the electron transfer must take place from another IBO to complete the overall HAA (recalling that this is a concerted reaction). As shown in Figure 6(f), in the vicinity of the TS-geometry, it is a β-IBO of the aryl π-cloud of Ar^2OH that evolves into a copper $d_{x^2-y^2}$ orbital. As the transfer of the proton and electron involve different donor/acceptor centers, this process is best described as a cPCET pathway, as indicated with curly arrows in Figure 7(b).

Continuing with the IBO analysis, a scenario similar to 1/Ar^{2}OH is present for the reaction of 3 with DHA, i.e., both α- and β-IBOs of the C–H bond remain on the hydrocarbon substrate (Figure 6(h) for β-IBO, Figure S24 for α-variant). Interestingly, a β-IBO of DHA π-density is found to evolve into a Cu $d_x{}^2–y^2$ orbital through a ligand-assisted pathway (Figure 6(i)), that is, density in a ligand π-IBO flows to Cu concomitantly with density from a DHA π-IBO flowing to the ligand itself. While this $\pi–\pi$ communication adds an additional layer of complexity with respect to detail, the overall electron flow makes it clear that the reaction of 3 with DHA is best described as a cPCET mechanism (Figure 7(c)), consistent with the conclusions drawn from analysis of projected dipole moment changes discussed above. IBO transformations of the remaining pairs: 2/DHA, 2/Ar^{2}OH, and 3/Ar^{2}OH are presented in the SI (Figures S21–S23). The net conclusion from these analyses is that 1–3 all react with Ar^{2}OH via a cPCET mechanism, 1 and 2 react with DHA via an HAT mechanism, but 3 instead abstracts a H-atom from DHA following the cPCET pathway.

In regard to details within the paradigm of a cPCET process, a varying degree of asynchronicity in H$^+$/e$^-$ transfer is possible during the concerted event, which can have a significant impact on the reaction rate. Hence, it is informative to be able to quantify the extent to which transfer of proton and electron coupled. One way to quantify this is to calculate the asynchronicity factor (η), a thermodynamic parameter introduced by Srnec and co-workers for describing the relative contributions of two competing factors dictating a net HAA process: the acidity constant (pK_a) and the redox potential.[36] In cases where acidobasic contributions are more important, a negative value of η is expected, while a positive value of η indicates a more dominant role of the redox potential.[13,36] For instance, it has been demonstrated recently that C–H bond activation by a Co(III)–oxo species with various hydrocarbons occurs via a *basic* asynchronous concerted pathway, where a H$^+$ is transferred to the acceptor-site prior to e$^-$ transfer (cf. Scheme 1).[13] The asynchronicity factor was computed to be *negative* in this case. The 3/DHA reactivity revealed here, by contrast, is concerted, but we compute it to be *oxidatively* asynchronous as we compute a *positive* value for η (+626 and +933 mV for reactions with Ar^{2}OH and DHA, respectively; Table S7).

A more visual picture of the oxidative asynchronicity in 3/DHA could be obtained by examining Figure 6(i2), which shows the electron-transfer event occurring at a point along the reaction coordinate where the H$^+$ is still primarily on the DHA fragment, consistent with an asynchronous cPCET mechanism having a more ET-like character in the TS. A comparative analysis of the cPCET mechanisms in 1/Ar^{2}OH and 3/DHA is provided in Figure 8, where evolution of the Hirshfeld spin population along the H-coordinate for both systems is plotted. Interestingly, for 3/DHA, the spin-density on the Cu-fragment starts increasing (and, that of the DHA moiety starts decreasing) well before the TS is reached— indicating early transfer of the electron from the substrate. This transfer is advanced even when comparing to the cPCET case of 1/Ar^{2}OH, where a similar change in density begins to appear only in close vicinity to the TS, in spite of the more polar character of the O–H bonds involved. This variation may presumably again be attributed to the substantially more positive standard reduction potential of 3 compared to 1 and 2.

CONCLUSIONS

A new $[Cu(III)-Y]^{2+}$ species with $Y = O_2CAr^1$(3) has been prepared and characterized. Its reactivity toward X–H bond (X = C, O) activation has been studied and compared to that of two analogous $[Cu(III)-Y]^{2+}$ cores with Y = OH (1) and OOCm (2) supported by the same L^{2-} ligand. Systematic comparison of reactivity with a given substrate across the series (Y = OH, OOCm, and O_2CAr^1) has enabled us to discern the contribution of the acceptor Y-group toward the complex's X–H bond functionalization reactivity. One key finding is that 3 is a better oxidant than 2 owing to the weaker carboxylate donor, which makes the Cu-center in 3 more electrophilic, and this in turn makes benzoate 3 more reactive than alkylperoxo 2. On the other hand, the greater basicity of the hydroxide moiety in 1 contributes significantly to its highest reactivity.

There are other mechanistic differences as well: detailed examination of X–H bond activation by 1–3 indicates variations in the synchronicity of concerted proton and electron transfer (CPET), ranging from quite asynchronous to the near-perfect synchronicity of true hydrogen-atom transfer, with reaction coordinates sensitive to both reactive ligand Y and substrate. Measurement of the dipole moment component projected on the H-donor/acceptor axis[16] proves one efficient means to assess relative synchronicity. Analysis of intrinsic bond orbitals[12,37,38] enables direct visualization of electron flow along reaction coordinates, and has been used here to resolve a mechanistic dichotomy within the paradigm of CPET reactions. For Y = OH and OOCm, reactions with 9,10-dihydroanthracene are found to proceed by hydrogen-atom transfer, while reactions with a bulky phenol are found to proceed instead by concerted proton-coupled electron transfer. For $Y = O_2CAr^1$, by contrast, *both* reactions are found to proceed by concerted proton-coupled electron transfer, with a high degree of oxidative asynchronicity, driven in part by the greater oxidizing power of the Cu(III) species. Such a detailed mechanistic picture delineating the coupled nature of proton and electron transfer from the substrate to different copper–oxygen species should be of broader relevance in HAA catalysis and can be exploited for strategic tuning of reactivity and selectivity toward various substrate X–H bonds.

Supplementary Material

Refer to Web version on PubMed Central for supplementary material.

ACKNOWLEDGMENTS

REFERENCES

(1). Solomon EI; Heppner DE; Johnston EM; Ginsbach JW; Cirera J; Qayyum M; Kieber-Emmons MT; Kjaergaard CH; Hadt RG; Tian L Copper Active Sites in Biology. Chem. Rev 2014, 114, 3659–3853. [PubMed: 24588098]

(2). (a)Lee JY; Karlin KD Elaboration of Copper–Oxygen Mediated C–H Activation Chemistry in Consideration of Future Fuel and Feedstock Generation. Curr. Opin. Chem. Biol 2015, 25, 184–193. [PubMed: 25756327] (b)Trammell R; D'Amore L; Cordova A; Polunin P; Xie N; Siegler MA; Belanzoni P; Swart M; Garcia-Bosch I Directed Hydroxylation of sp^2 and sp^3 C–H Bonds Using Stoichiometric Amounts of Cu and H_2O_2. Inorg. Chem 2019, 58, 7584–7592. [PubMed: 31084018]

(3). (a)Itoh S Developing Mononuclear Copper–Active-Oxygen Complexes Relevant to Reactive Intermediates of Biological Oxidation Reactions. Acc. Chem. Res 2015, 48, 2066–2074. [PubMed: 26086527] (b)Liu JJ; Diaz DE; Quist DA; Karlin KD Copper(I)- Dioxygen Adducts and Copper Enzyme Mechanisms. Isr. J. Chem 2016, 56, 738–755.(c)Elwell CE; Gagnon NL; Neisen BD; Dhar D; Spaeth AD; Yee GM; Tolman WB Copper-Oxygen Complexes Revisited: Structures, Spectroscopy, and Reactivity. Chem. Rev 2017, 117, 2059–2107. [PubMed: 28103018]

(4). (a)Donoghue PJ; Tehranchi J; Cramer CJ; Sarangi R; Solomon EI; Tolman WB Rapid C–H Bond Activation by a Monocopper(III)–Hydroxide Complex. J. Am. Chem. Soc 2011, 133, 17602–17605. [PubMed: 22004091] (b)Dhar D; Yee GM; Markle TF; Mayer JM; Tolman WB Reactivity of the copper(III)-hydroxide unit with phenols. Chem. Sci 2017, 8, 1075–1085. [PubMed: 28572905] (c)Dhar D; Tolman WB Hydrogen Atom Abstraction from Hydrocarbons by a Copper(III)- Hydroxide Complex. J. Am. Chem. Soc 2015, 137, 1322–1329. [PubMed: 25581555] (d)Neisen BD; Gagnon NL; Dhar D; Spaeth AD; Tolman WB Formally Copper(III) −Alkylperoxo Complexes as Models of Possible Intermediates in Monooxygenase Enzymes. J. Am. Chem. Soc 2017, 139, 10220–10223. [PubMed: 28722408] (e)Bailey WD; Dhar D; Cramblitt AC; Tolman WB Mechanistic Dichotomy in Proton-Coupled Electron-Transfer Reactions of Phenols with a Copper Superoxide Complex. J. Am. Chem. Soc 2019, 141, 5470–5480. [PubMed: 30907590]

(5). (a)Dhar D; Yee GM; Spaeth AD; Boyce DW; Zhang H; Dereli B; Cramer CJ; Tolman WB Perturbing the Copper(III)–Hydroxide Unit through Ligand Structural Variation. J. Am. Chem. Soc 2016, 138, 356–368. [PubMed: 26693733] (b)Dhar D; Yee GM; Tolman WB Effects of Charged Ligand Substituents on the Properties of the Formally Copper(III)-Hydroxide [CuOH]$^{2+}$) Unit. Inorg. Chem 2018, 57, 9794–9806. [PubMed: 30070473]

(6). (a)Ackermann L Carboxylate-Assisted Transition-Metal-Catalyzed C–H Bond Functionalizations: Mechanism and Scope. Chem. Rev 2011, 111, 1315–1345. [PubMed: 21391562] (b)Shi G; Zhang Y Carboxylate-Directed C-H Functionalization. Adv. Synth. Catal 2014, 356, 1419–1442. (c)Davies DL; Macgregor SA; McMullin CL Computational Studies of Carboxylate-Assisted C-H Activation and Functionalization at Group 8–10 Transition Metal Centers. Chem. Rev 2017, 117, 8649–8709. [PubMed: 28530807] (d)Afreen F; Mathur P; Rheingold A Oxidase Studies of Some Benzimidazole Diamide Copper(II) Complexes. Inorg. Chim. Acta 2005, 358, 1125–1134.

(7). Such reactivity has been reported for Ni complexes:Pirovano P; Farquhar ER; Swart M; McDonald AR Tuning the Reactivity of Terminal Nickel(III)-Oxygen Adducts for C-H Bond Activation. J. Am. Chem. Soc 2016, 138, 14362–14370. [PubMed: 27739688]

(8). Weinberg DR; Gagliardi CJ; Hull JF; Murphy CF; Kent CA; Westlake BC; Paul A; Ess DH; McCafferty DG; Meyer TJ Proton-coupled electron transfer. Chem. Rev 2012, 112, 4016–4093. [PubMed: 22702235]

(9). Warren JJ; Tronic TA; Mayer JM Thermochemistry of Proton-Coupled Electron Transfer Reagents and Its Implications. Chem. Rev 2010, 110, 6961–7001. [PubMed: 20925411]

(10). Hodgkiss JM; Rosenthal J; Nocera DG The Relation between Hydrogen Atom Transfer and Proton-Coupled Electron Transfer in Model Systems In Hydrogen-Transfer Reactions; Hynes JT, Klinman JP, Limbach H-H, Schowen RL, Eds.; Wiley-VCH Verlag GmbH: Weinheim, 2007; pp 503–562.

(11). (a)Hammes-Schiffer S Theoretical Perspectives on Proton Coupled Electron Transfer Reactions. Acc. Chem. Res 2001, 34, 273– 281. [PubMed: 11308301] (b)Cukier RI Theory and Simulation of Proton-Coupled Electron Transfer, Hydrogen-Atom Transfer, and Proton Translocation in Proteins. Biochim. Biophys. Acta, Bioenerg 2004, 1655, 37–44.

(12). Klein JEMN; Knizia G cPCET versus HAT: A Direct Theoretical Method for Distinguishing X-H Bond-Activation Mechanisms. Angew. Chem., Int. Ed 2018, 57, 11913–11917.

(13). Goetz MK; Anderson JS Experimental Evidence for pKa-Driven Asynchronicity in C−H Activation by a Terminal Co(III)− Oxo Complex. J. Am. Chem. Soc 2019, 141, 4051–4062. [PubMed: 30739450]

(14). (a)Usharani D; Lacy DC; Borovik AS; Shaik S Dichotomous Hydrogen Atom Transfer vs Proton-Coupled Electron Transfer during Activation of X-H Bonds (X = C, N, O) by Nonheme Iron-Oxo Complexes of Variable Basicity. J. Am. Chem. Soc 2013, 135, 17090–17104. [PubMed: 24124906] (b)Geng C; Weiske T; Li J; Shaik S; Schwarz H Intrinsic Reactivity of Diatomic 3d Transition-Metal Carbides in the Thermal Activation of Methane: Striking Electronic Structure Effects. J. Am. Chem. Soc 2019, 141, 599–610. [PubMed: 30520302]

(15). (a)Hammes-Schiffer S Proton-Coupled Electron Transfer: Moving Together and Charging Forward. J. Am. Chem. Soc 2015, 137, 8860–8871. [PubMed: 26110700] (b)Hammes-Schiffer S; Stuchebrukhov AA Theory of Coupled Electron and Proton Transfer Reactions. Chem. Rev 2010, 110, 6939–6960. [PubMed: 21049940]

(16). (a)Soudackov AV; Hammes-Schiffer S Probing Non-adiabaticity in the Proton-Coupled Electron Transfer Reaction Catalyzed by Soybean Lipoxygenase. J. Phys. Chem. Lett 2014, 5, 3274–3278. [PubMed: 25258676] (b)Sirjoosingh A; Hammes-Schiffer S Proton-Coupled Electron Transfer versus Hydrogen Atom Transfer: Generation of Charge-Localized Diabatic States. J. Phys. Chem. A 2011, 115, 2367–2377. [PubMed: 21351757] (c)Muñoz-Rugeles L; Alvarez-Idaboy JR A Proton−Electron Sequential Transfer Mechanism: Theoretical Evidence about Its Biological Relevance. Phys. Chem. Chem. Phys 2015, 17, 28525–28528. [PubMed: 26456543]

(17). Yang L; Powell DR; Houser RP Structural Variation in Copper(I) Complexes with Pyridylmethylamide Ligands: Structural Analysis with a New Four-Coordinate Geometry Index, τ_4. Dalton Trans. 2007, No. 9, 955–964. [PubMed: 17308676]

(18). Connelly NG; Geiger WE Chemical Redox Agents for Organometallic Chemistry. Chem. Rev 1996, 96, 877–910. [PubMed: 11848774]

(19). Complex 3 reacts with TEMPOH with a second-order rate constant of 5.8(2) × 103 M^{-1} s^{-1} at −80 °C in THF (KIE = 2.6) (measured using stopped-flow kinetics, see Figures S15–S17), which is 2 orders of magnitude faster than the same reaction of 2 (2.4 $M^{-1}s^{-1}$, ref 4d) but is slower than the reaction of 1, which is too fast to be measured accurately. Because of this latter problem, we focus here instead on slower reactions with Ar^3OH and DHA.

(20). Brigati G; Lucarini M; Mugnaini V; Pedulli GF Determination of the Substituent Effect on the O−H Bond Dissociation Enthalpies of Phenolic Antioxidants by the EPR Radical Equilibration Technique. J. Org. Chem 2002, 67, 4828–4832. [PubMed: 12098294]

(21). Maeder M; King P Reactlab; Jplus Consulting Pty, Ltd.: East Freemantle, WA. Australia, 2009.

(22). Ferguson J; Reeves LW; Schneider WG Vapor Absorption Spectra and Oscillator Strengths of Naphthalene, Anthracene and Pyrene. Can. J. Chem 1957, 35, 1117–1123.

(23). Comparison of the rate of decay of 3 upon treatment with DHA and DHA-d_4 (−25 °C, 500 equiv, 1,2-DFB) revealed a k_H/k_D of ~62.$_{4HD}$

(24). (a)Becke AD Density-Functional Thermochemistry. III. The Role of Exact Exchange. J. Chem. Phys 1993, 98, 5648–5652.(b)Becke AD Density-functional Thermochemistry. IV. A New Dynamical Correlation Functional and Implications for Exact exchange Mixing. J. Chem. Phys 1996, 104, 1040–1046.

(25). (a)Grimme S; Ehrlich S; Goerigk L Effect of the Damping Function in Dispersion Corrected Density Functional Theory. J. Comput. Chem 2011, 32, 1456–1465. [PubMed: 21370243] (b)Johnson ER; Becke AD A Post-Hartree-Fock Model of Intermolecular Interactions: Inclusion of Higher-Order Corrections. J. Chem. Phys 2006, 124, 174104. [PubMed: 16689564]

(26). Hehre WJ; Ditchfield R; Pople JA Self-Consistent Molecular Orbital Methods. XII. Further Extensions of Gaussian Type Basis Sets for Use in Molecular Orbital Studies of Organic Molecules. J. Chem. Phys 1972, 56, 2257–2261.

(27). Dolg M; Wedig U; Stoll H; Preuss H Energy-adjusted Ab Initio Pseudopotentials for the First Row Transition Elements. J. Chem. Phys 1987, 86, 866–872.

(28). Weigend F; Ahlrichs R Balanced Basis Sets of Split Valence, Triple Zeta Valence and Quadruple Zeta Valence Quality for H to Rn: Design and Assessment of Accuracy. Phys. Chem. Chem. Phys 2005, 7, 3297–3305. [PubMed: 16240044]

(29). Marenich AV; Cramer CJ; Truhlar DG Universal Solvation Model Based on Solute Electron Density and on a Continuum Model of the Solvent Defined by the Bulk Dielectric Constant and Atomic Surface Tensions. J. Phys. Chem. B 2009, 113, 6378–6396. [PubMed: 19366259]

(30). Adamo C; Barone V Toward Reliable Density Functional Methods without Adjustable Parameters: The PBE0Model. J. Chem. Phys 1999, 110, 6158–6170.

(31). Dereli B; Momeni MR; Cramer CJ Density Functional Modeling of Ligand Effects on Electronic Structure and C–H Bond Activation Activity of Copper(III) Hydroxide Compounds. Inorg. Chem 2018, 57, 9807–9813. [PubMed: 30070468]

(32). Kitagawa Y; Saito T; Ito M; Nakanishi Y; Shoji M; Koizumi K; Yamanaka S; Kawakami T; Okumura M; Yamaguchi K Geometry Optimization Method Based on Approximate Spin Projection and Its Application to F_2, CH_2, CH_2OO, and Active Site of Urease. Int. J. Quantum Chem 2007, 107, 3094–3102.

(33). Szabo A; Ostlund NS Modern Quantum Chemistry; Dover Publications: New York, 1996; Chapter 3, p 205.

(34). Yamaguchi K; Takahara Y; Fueno T; Houk KN Extended Hartree-Fock (EHF) Theory of Chemical Reactions. Theor. Chim. Acta 1988, 73, 337–364.

(35). Stowasser R; Hoffmann R What Do the Kohn-Sham Orbitals and Eigenvalues Mean? J. Am. Chem. Soc 1999, 121, 3414.

(36). Bím D; Maldonado-Domínguez M; Rulíšek L; Srnec M Beyond the Classical Thermodynamic Contributions to Hydrogen Atom Abstraction Reactivity. Proc. Natl. Acad. Sci. U. S. A 2018, 115, E10287–E10294. [PubMed: 30254163]

(37). Knizia G Intrinsic Atomic Orbitals: An Unbiased Bridge between Quantum Theory and Chemical Concepts. J. Chem. Theory Comput 2013, 9, 4834–4843. [PubMed: 26583402]

(38). (a)Knizia G; Klein JEMN Electron Flow in Reaction Mechanisms-Revealed from First Principles. Angew. Chem., Int. Ed 2015, 54, 5518–5522.(b)Ching W-M; Zhou A; Klein JEMN; Fan R; Knizia G; Cramer CJ; Guo Y; Que L Characterization of the Fleeting Hydroxoiron(III) Complex of the Pentadentate TMC-Py Ligand. Inorg. Chem 2017, 56, 11129–11140. [PubMed: 28858496]
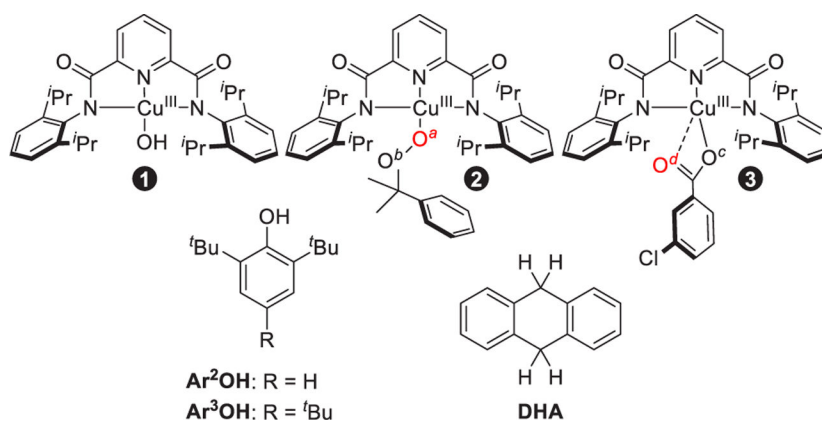
Figure 1.

Two organic substrates, DHA and Ar^{n}OH ($n = 2$ in theoretical studies, $n = 3$ in experimental studies), used in this study together with three [LCu(III)−Y] complexes. The a,a-dimethylbenzyl group in 2 is abbreviated as "Cm" and the *meta*-chlorophenyl group in 3 is referred to as "Ar^1".
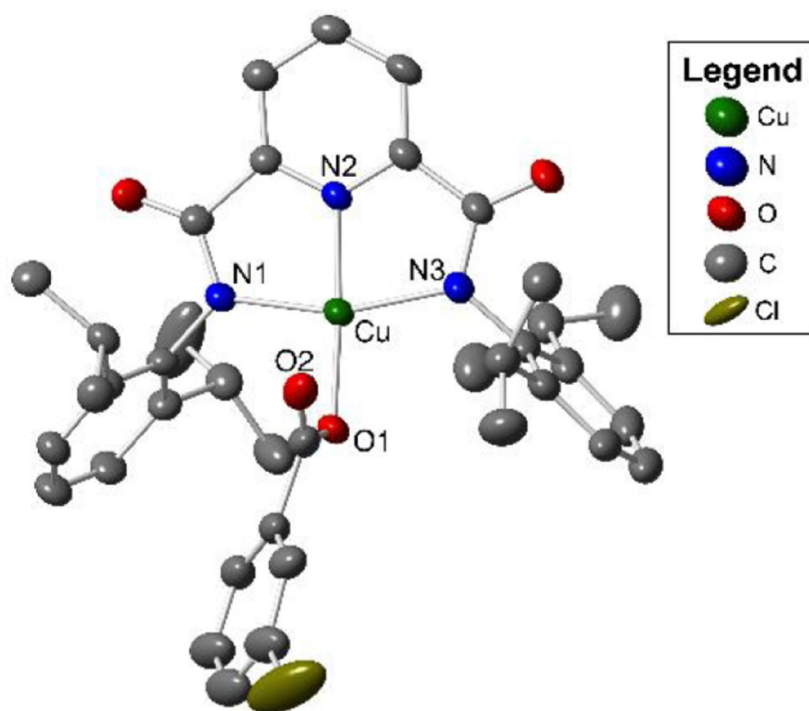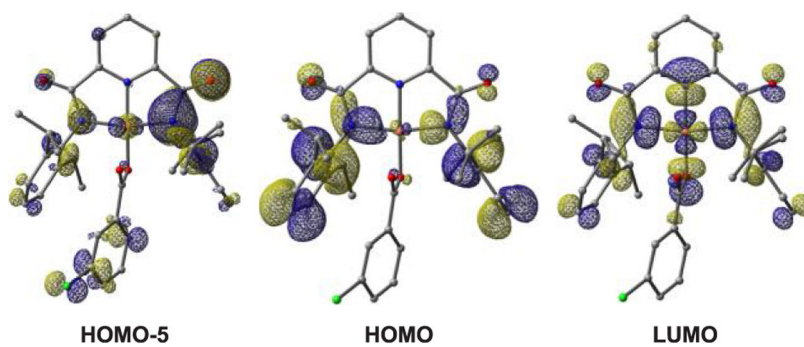
Figure 2.
X-ray crystal structure of anionic 3′ with the NEt₄ cation and H atoms omitted for clarity. All non-hydrogen atoms are shown as 50% thermal ellipsoids. Selected interatomic distances (Å) and angles (deg): Cu−O1, 1.929(3); Cu−O2, 2.516(3); Cu−N1, 2.005(3); Cu−N2, 1.912(3); Cu−N3, 2.018(3); N1−Cu−N3, 160.44(13); N1−Cu−N2, 80.48(12); N2−Cu−O1, 176.17(12).
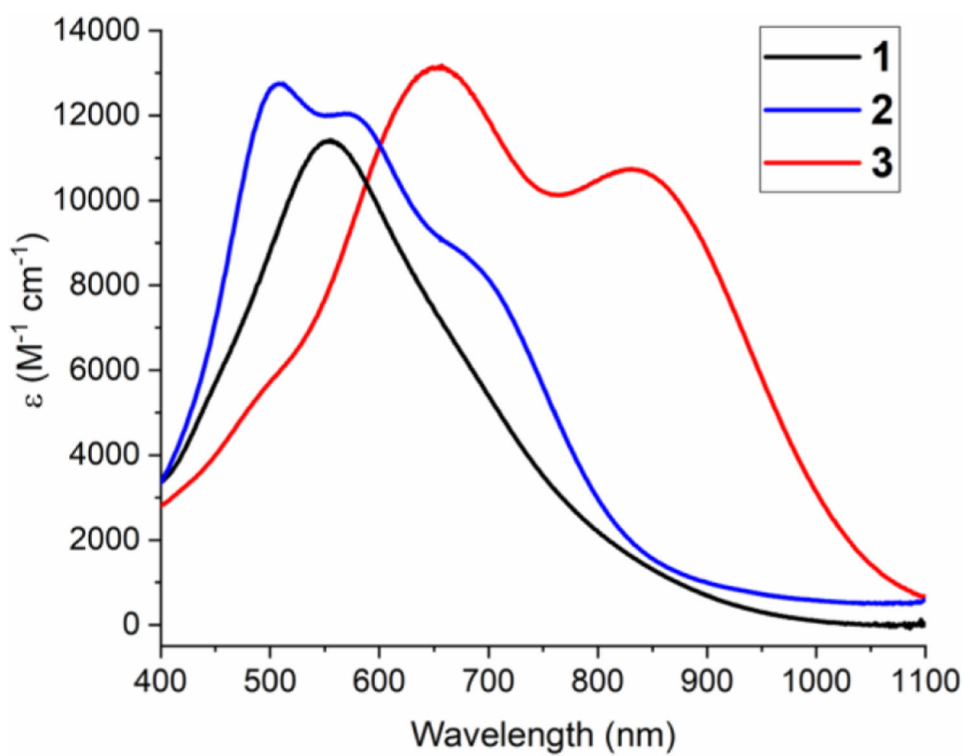
Figure 3.
Overlay of UV−vis spectra of LCu(III)OH (1, black), LCu(III)OOCm (2, blue), and
LCu(III)O$_2$CAr^1(3, red), in THF at−80 °C.

HOMO-5   **HOMO**   **LUMO**

Figure 4.
Spectroscopically relevant highest occupied molecular orbital (HOMO) and HOMO−5, together with the lowest unoccupied molecular orbital (LUMO) for complex 3.
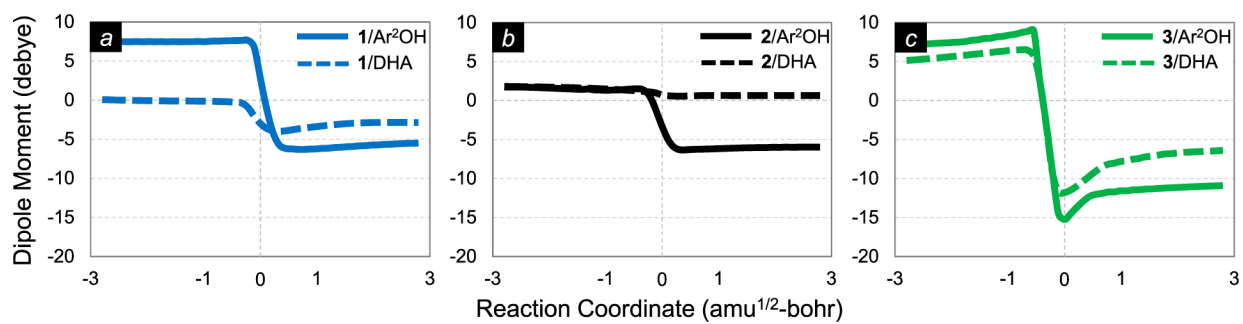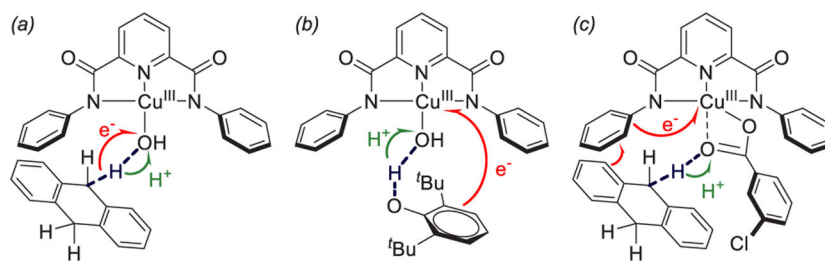
Figure 5.
Evolution of the total dipole moment vector (Hirshfeld) projected along the axis of H-atom abstraction. (a), (b), and (c) correspond to HAA reactivity of complexes 1 (blue), 2 (black), and 3 (green), respectively. Solid lines are used for the Ar^2OH substrate, while dashed-lines represent the DHA substrate.
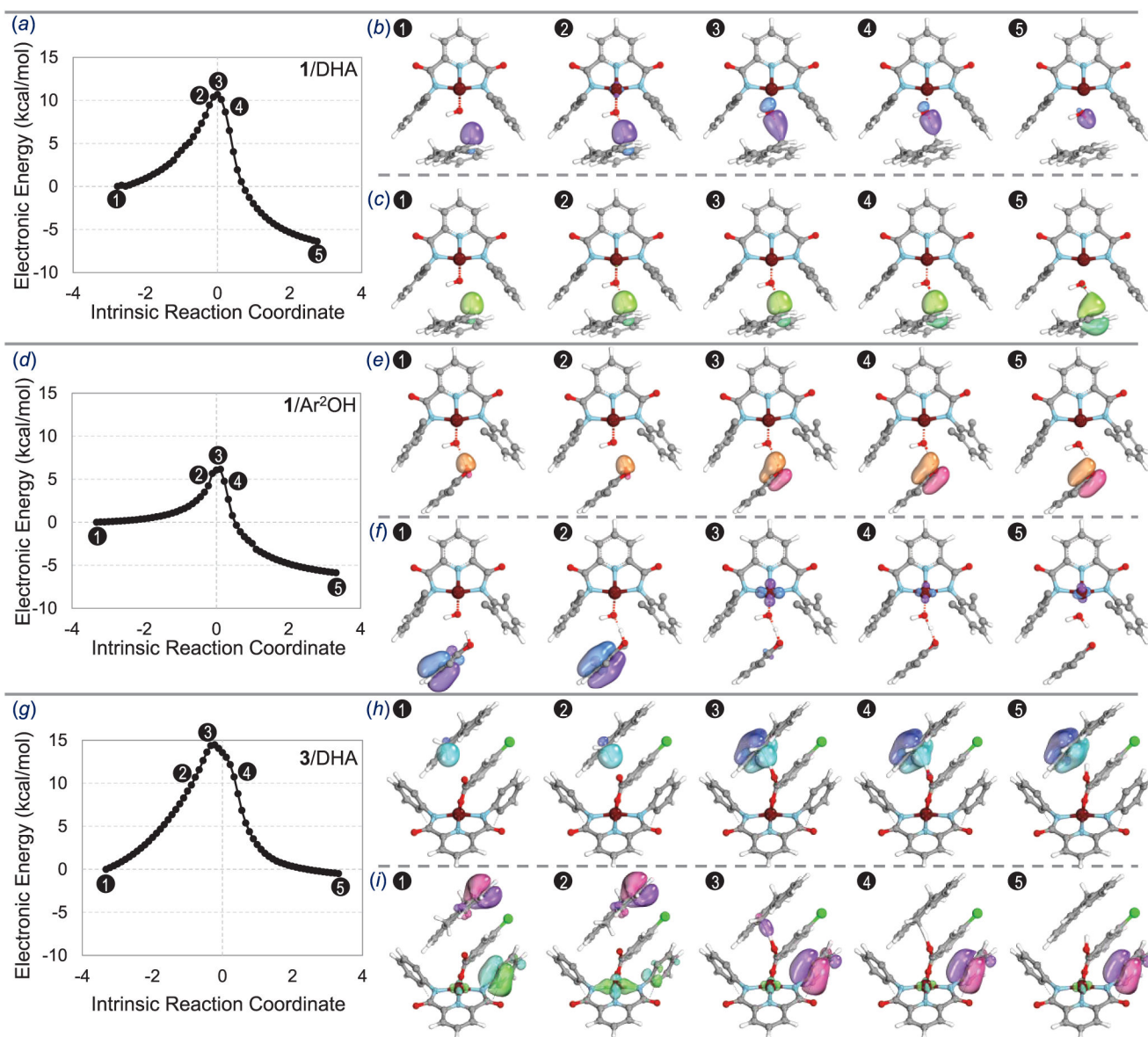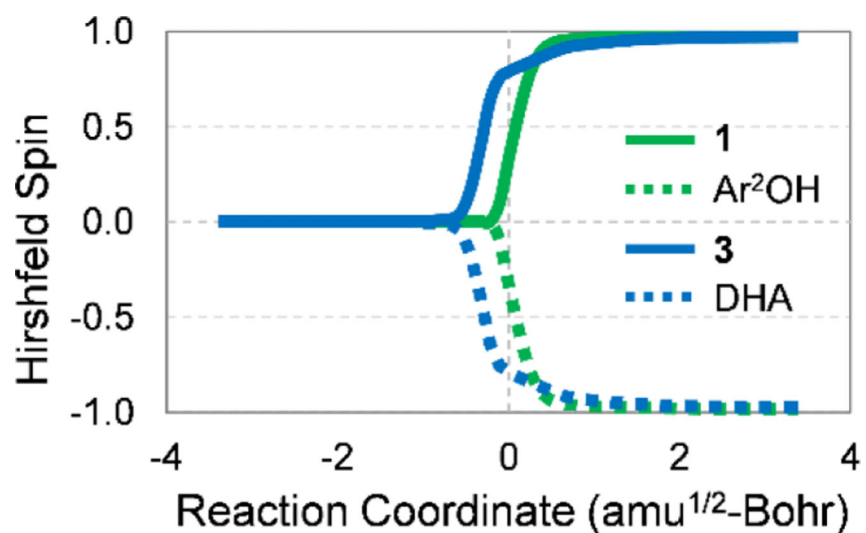
Figure 6.
Plots of the change in electronic energies (computed at UB3LYP-D3(BJ)/basis-I level) along the intrinsic reaction coordinate (IRC/amu$^{1/2}$-bohr) for (a) 1/DHA, (d) 1/Ar^{2}OH, and (g) 3/DHA pairs. Intrinsic bond orbital (IBO) transformations of the C–H bond along the IRC are shown in (b) purple (α-IBO) and (c) green (β-IBO). Changes in the O–H β-IBO for 1/Ar^{2}OH are shown in (e), while (f) shows changes in the β-IBO of the π-electron density of the aryl ring that eventually ends up on the Cu-atom. Transformation of the C–H β-IBO for 3/DHA is presented in (h), with the density remaining on the DHA moiety. Changes in two β-IBOs corresponding to the π-density of DHA (blue-green) and that of the diisopropylphenyl moiety of the ligand (pink-orange) are represented simultaneously in (i). IBO transformations indicate that the density on DHA is transferred to the Cu-center through a ligand-assisted pathway. In all cases, isopropyl groups of the ligand and *tert*-butyl groups of the Ar^{2}OH substrate are omitted for clarity.

Figure 7.
Electron flow during HAA from (a) 1/DHA, (b) 1/Ar^{2}OH, and (c) 3/DHA.

Figure 8.
Changes in the Hirshfeld spin-population for 1/Ar^{2}OH (green) and 3/DHA (blue), along their respective cPCET reaction coordinates. Solid lines represent total spin on Cu-complexes (Fragment^{Cu}), while dotted lines reflect the total spin on organic substrates (Fragment^{Sub}). At the start of the reaction, both Fragment^{Cu} and Fragment^{Sub} are closed-shell systems, thus the total spin on both fragments starts from zero. At/near the TS, single electron transfer leads to local spin on both fragments.
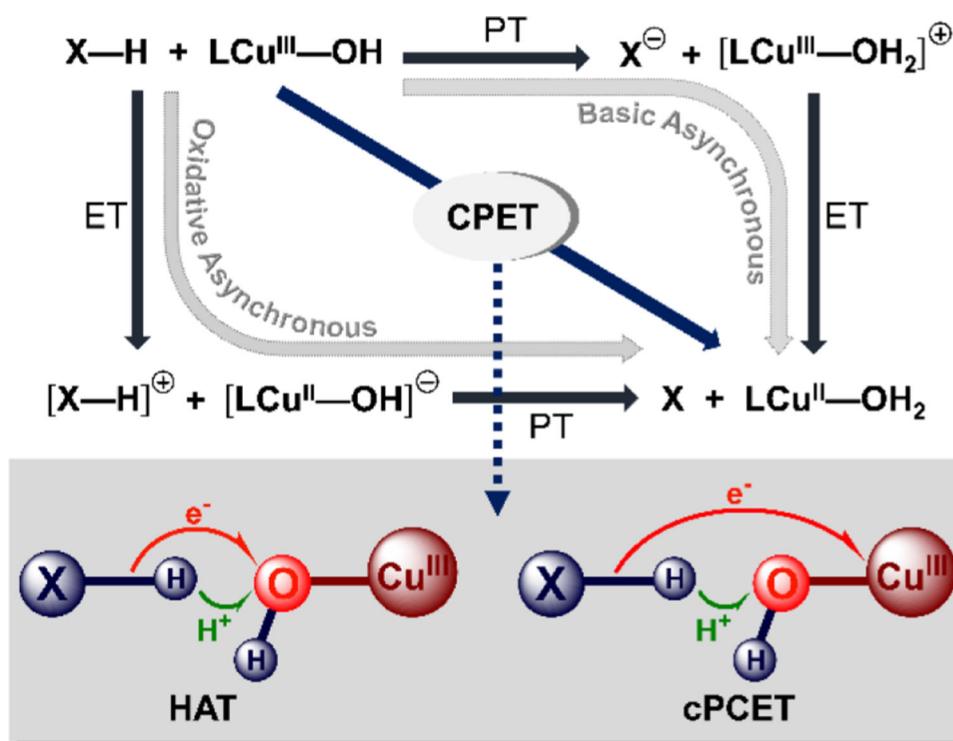
Scheme 1.
Stepwise (ET/PT or PT/ET) vs CPET Pathways for X−H Bond Activation by a Representative Cu(III) Species (1)[a]

[a]Two key variations of CPET reaction, namely, HAT and cPCET, are also shown.
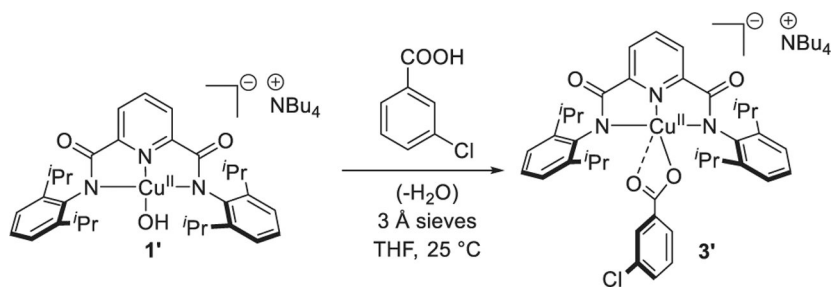
Scheme 2.
Synthesis of [NBu$_4$][LCu(II)O$_2$Car^1], **3′**, Starting from [NBu$_4$][LCu(II)OH)], **1′**

Table 1.

Experimental Second Order Rate Constants (k_2, M^{-1} s^{-1}) for HAA from Ar^3OH[a] and DHA[b] with Complexes 1–3

species	Ar^3OH	DHA
1	$2(1) \times 10^1$	$4.2(9) \times 10^1$
2	*no rxn.*	*no rxn.*
3	$3(1) \times 10^{-1}$	$1.1(4) \times 10^{-1}$

[a]Measured at −80 °C in THF.

[b]Measured at −25 °C in 1,2-DFB.

Table 2.

Most Intense Molecular Excitation Energies Computed[a] for Different Cu(III) Complexes[b]

species	orbital energy (eV)		excitation energies (eV)
	HOMO	**LUMO**	
1	−6.49	−3.59	2.24 (2.30)
2	−6.36	−3.72	1.78 (1.76), 2.06 (2.14), 2.80 (2.48)
3	−6.42	−3.99	1.63 (1.49), 1.90 (1.91), 2.65 (2.53)

[a]TD-DFT calculations performed at PBE0-D3(BJ)/basis-III/SMD-(THF)//B3LYP-D3(BJ)/basis-I level of theory.

[b]Experimental excitation energies are provided in parentheses for comparison.

Table 3.

Free Energies of Activation ($\Delta G^{\ddagger}$, kcal/mol) Calculated for Different Reactive Sites O^a, O^b, O^c, or O^d with Ar^2OH and DHA Substrates[a]

species	Ar^2OH ($\Delta G^{\ddagger}_{193}$)	DHA ($\Delta G^{\ddagger}_{248}$)
2 (O^a)	8.0	16.8
2 (O^b)	21.2	23.2
3 (O^c)	11.6	19.0
3 (O^d)	2.9	14.5

[a] B3LYP-D3(BJ)/basis-I/SMD(solvent)//B3LYP-D3(BJ)/basis-I at 193.15 K for Ar^2OH and 248.15 K for DHA.

Table 4.

Computed[a] Free Energies of Activation ($\Delta G^{\ddagger}$, kcal/mol) for HAA from Ar^2OH and DHA with Complexes 1−3

species	Ar^2OH ($\Delta G^{\ddagger}_{193}$)	DHA ($\Delta G^{\ddagger}_{248}$)
1	2.6	7.0
2 (O^a)	8.0	16.8
3 (O^d)	2.9	14.5

[a]B3LYP-D3(BJ)/basis-I/SMD(solvent)//B3LYP-D3(BJ)/basis-I level of theory at 193.15 K for Ar^2OH and at 248.15K for DHA.